I&EC research
Industrial & Engineering Chemistry Research

ARTICLE

pubs.acs.org/IECR

4-Chlorophenol Oxidation Photocatalyzed by a Calcined Mg−Al−Zn Layered Double Hydroxide in a Co-current Downflow Bubble Column

Eduardo Martín del Campo,[†] Jaime Sanchez Valente,[‡] Thelma Pavón,[§] Rubí Romero,[†] Ángeles Mantilla,[▽] and Reyna Natividad[†,*,⊥]

[†]Centro Conjunto de Investigación en Química Sustentable, Universidad Autónoma del Estado de México, Km 14.5 Carretera Toluca−Atlacomulco, México

[‡]Instituto Mexicano del Petróleo, Eje Central #152, México D. F., 07730

[§]Facultad de Química, Universidad Autónoma del Estado de México, Paseo Colon esq. Paseo Tollocan, Toluca, Estado de México, 50120

[▽]CICATA-LEGARIA, Instituto Politécnico Nacional, Av. Legaria #694, México D. F., 11500

ABSTRACT: The objective of this work is to study, for the first time, the photodegradation of 4-chlorophenol (4CP) catalyzed by a calcined Mg−Zn−Al layered double hydroxides (MgAlZn LDHs) in a co-current downflow bubble column (CDBC) photoreactor at pilot scale. The effect of initial organic compound concentration (C_{4CP0}), temperature (T), and mass catalyst over reaction rate ($-r_{4CP}$) was elucidated. An intrinsic kinetic regime was established, and a single-site Langmuir−Hinshelwood mechanism was determined to occur during the organic compound oxidation. The catalyst was characterized by X-ray diffraction (XRD), inductively coupled plasma atomic emission spectrometry (ICP-AES), and ultraviolet−visible light (UV/vis) spectrophotometry. The reaction progress was verified by UV/vis spectrophotometry and total organic carbon (TOC) content. Degradation and mineralization rate were found to be dependent on T and 4CP concentration. In the range of studied operating conditions, a maximum of 94% 4CP was degraded, while 70% total organic carbon removal was achieved.

1. INTRODUCTION

Although environmental risks have always been a constant in chemical processes, it was not until the last decades of the 20th century that efforts to protect the environment were strengthened. Two general approaches may be identified. The first one is known as being corrective and implies the mineralization of industrial effluents to fulfill regulations, and the second one implies the development of sustainable processes (green chemistry). For both of them, photocatalysis has proven to play a major role since it allows one to carry out complete mineralization of organic compounds and selective oxidations under mild conditions (low temperature, atmospheric pressure, neutral pH). In this context, the photocatalyzed degradation of phenolic compounds has had priority and therefore has been widely studied, mainly with TiO_2. Among such organic compounds, chlorophenols (CPs) constitute a particular group of priority pollutants, because most of them are toxic, hardly biodegradable, and difficult to remove from the environment. The half-life for pentachlorophenols (PCPs) in water can reach 3.5 months in aerobic waters and some years in organic sediments. Because of their numerous origins (pesticides, insecticides, paper, and wood preservatives industry), CPs can be found in ground water, wastewater, and soil. They might produce a disagreeable taste and odor to drinking water at concentrations of <0.1 μg/L. The limiting permissible concentration of CPs in drinking water should not exceed 10 μg/L.[1] In particular, 4-chlorophenol (4CP) has been recognized as a precursor of highly toxic compounds. The photodegradation of such a compound has been reported mainly with TiO_2 and in stirred tank reactors at laboratory scale. In related literature,[2] a main concern is the low quantum efficiency attained as a consequence of a fast recombination of the generated hole−electron (h^+_{VB}/e^-_{CB}) pairs in the catalytic surface. A general accepted solution to this issue has been the addition of an electron acceptor such as oxygen. Then, a substantial responsibility for the success of a photo-oxidation process relies on the design of a reactor that allows the optimization of mass-transfer from gas to liquid. At this point, bubble columns, and specially the co-current downflow bubble column (CDBC), emerge as a promising technology to carry out the catalyzed photo-oxidation of effluents at the industrial scale. To accomplish such a purpose, it is of paramount importance to assess the performance of the CDBC at pilot scale first.

The co-current downflow contactor (CDC) or CDBC is a highly efficient mass-transfer device.[3] It consists of a bubble column, where the gas (dispersed phase) and liquid (continuous phase) are introduced co-currently through an orifice at the top of a fully flooded column. The hydrodynamic action of a high inlet liquid velocity, initiates and maintains a turbulent bubble matrix or gas−liquid dispersion, containing densely packed bubbles (gas holdup given as ε_G = 0.4−0.6) that undergo constant coalescence and breakup with a particular bubble diameter related to the system under consideration.[4] When a stable gas−liquid dispersion is accomplished, the turbulence, the mixing and shear give rise to a large gas−liquid interfacial area (a = 1000−6000 m^2/m^3, depending on bubble size) and, therefore,

Received: March 14, 2011
Accepted: August 21, 2011
Revised: July 29, 2011
Published: August 21, 2011

dx.doi.org/10.1021/ie200412p | *Ind. Eng. Chem. Res.* 2011, 50, 11544–11552

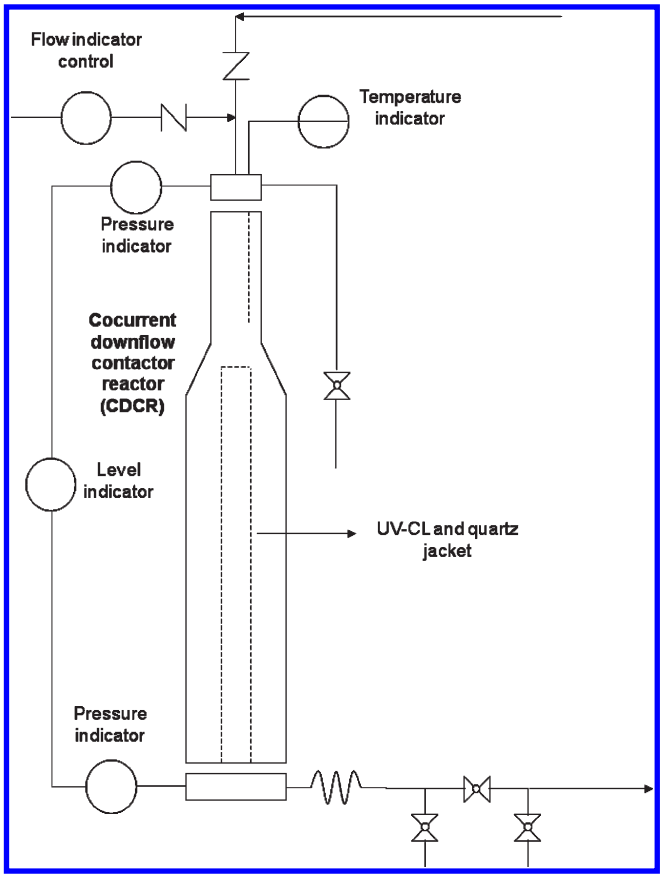

Figure 1. Schematic diagram of the CDBC.

a very high gas−liquid volumetric mass-transfer coefficient (k_La). Typical k_La values for the O_2/H_2O system are in the range of 0.25−1.5 s^{-1}.[5]

Because of the aforementioned characteristics, the CDBC has been employed in heterogeneous processes that include hydrogenation[6−9] and heterogeneous photocatalytic oxidation.[5,10,11] Regarding the latter, the CDBC has been used to efficiently carry out the photocatalytic oxidation of phenol,[12] 2,4,6-trichlorophenol (2,4,6TCP),[10] and 1,8-diazabicyclo[5,4,0]undec-7-ene (DBU)[11] in aqueous solutions with the extensively studied TiO_2 as a photocatalyst.

The increasing demand for solutions to the multiple environmental problems associated with the use of toxic compounds has led to a search for new alternatives in the use of novel compounds as photocatalysts. In this context, layered double hydroxides (LDHs) have emerged as important precursors of compounds that possess photocatalytic activity.[13−16] LDHs or hydrotalcite-like compounds (HLCs) are anionic clays. The structure of these inorganic materials is very similar to brucite $Mg(OH)_2$, in which each Mg cation is octahedrally surrounded by hydroxyls. Their chemical composition can be expressed by the general formula $M^{II}_{1-x}M^{III}_x(OH)_2A^{n-}_{x/n}\cdot yH_2O$, where M^{II} and M^{III} are divalent and trivalent metal cations, A^{n-} is an anion with a valency of n, and x is a portion of trivalent cations (usually $0.20 < x < 0.35$). These compounds have a layered crystal structure positively charged $[M^{II}_{1-x}M^{III}_x(OH)_2]^{x+}$, which is compensated by interlayer anions. At temperatures of ∼300−500 °C, HLCs are calcined to form mixed oxides of M^{II} and M^{III} metals (solids with basic properties).[17] Successful photocatalytic applications of calcined ZnAl,[18] ZnFeAl,[14,15] and MgAlZn[13] LDHs have been reported for the degradation of different organic compounds at laboratory scale. LDHs have many advantages over other materials, and there has been considerable interest in their use to remove contaminants at larger scales, because they are nontoxic, have low cost, and are easily prepared. However, the application of these compounds at different levels not only depends on their proven catalytic efficiency but also on the reactor design that may optimize their performance. Thus, the aim of this study was to evaluate the catalytic performance of hydrotalcite-like compounds (MgAlZn LDHs) in the photocatalyzed oxidation of an aromatic compound (4CP) under high gas−liquid−solid mass-transfer conditions achieved in a CDBC at pilot scale.

2. EXPERIMENTAL SECTION

2.1. Experimental Setup: The CDBC. To carry out the present study, it was necessary to assemble a CDBC that was constructed with QVF glass and fittings, coupled with a HI-TECH NNI 400/147 XL UV−C lamp (UV-CL), which was encased by a quartz jacket, and the entire piping system was composed of 304 stainless steel (304 SS). Figure 1 depicts the CDBC setup.

The CDBC consists of two sections; the upper section (high mass-transfer zone) is a cylindrical column with an internal diameter of 0.05 m (nominally 50 mm) and a length of 0.475 m. In this zone, a vigorously agitated gas−liquid dispersion is created due to the energy and intense turbulence introduced by the high inlet liquid velocity. The lower section (bubble disengagement/heterogeneous photocatalytic reaction zone) is a cylindrical column with an internal diameter of 0.076 m (nominally 80 mm) and a length of 1.5 m. The CDBC was operated in semibatch mode (continuous supply of gas phase), where the liquid stream containing reactants was recirculated with the aid of a centrifugal turbine pump. Table 1 shows the principal operating parameters of the CDBC.

2.2. Catalyst Synthesis and Characterization. Powders of MgAlZn LDHs containing 5 wt % of Zn (MgAlZn−5% LDHs) were synthesized by the coprecipitation method at constant pH.[13] This percentage of Zn was chosen because, in a previous study,[13] calcined MgAlZn LDHs with different amounts of Zn were prepared and tested in the photocatalytic degradation of phenol, a high photocatalytic activity was observed for calcined MgAlZn−5% LDHs, degrading ∼70% of phenol.[13] To synthesize MgAlZn−5% LDHs, an aqueous solution (solution M) containing dissolved salts of $Mg(NO_3)_2\cdot 6H_2O$, $Zn(NO_3)_2\cdot 6H_2O$ and $Al(NO_3)_3\cdot 9H_2O$ in deionized (DI) water was prepared. Molar concentrations of these salts were 0.76, 0.07, and 0.38 M, respectively. At the same time, an aqueous alkaline solution (solution A) was prepared containing KOH and K_2CO_3 in DI water with a molar concentration of 1.33 and 0.66 M, respectively. Solutions M and A were added simultaneously and slowly to a 5×10^{-3} m^3 glass reactor, containing 5×10^{-4} m^3 of DI water. This resulted in the formation of a precipitate. The so obtained precipitate was kept under mechanical stirring at 60 °C for 18 h. Afterward, products were thoroughly washed with distilled and DI water in order to eliminate excess ions. Finally, the product was dried at 100 °C for 24 h.

Powders of MgAlZn−5% LDHs were analyzed by X-ray diffraction (XRD) in a Bruker D8 Advanced diffractometer with Cu Kα radiation and a Lynxeye detector. The specific analysis condition were: 30 kV, 25 mA, diffraction intensity was measured between 5° and 8° 2θ, with a 2θ step of 0.02°, and a counting time of 31.8 s. Subsequently, solids were calcined at 500 °C for

dx.doi.org/10.1021/ie200412p |Ind. Eng. Chem. Res. 2011, 50, 11544–11552

Table 1. CDBC Operating Parameters

CDBC volume, V_{CDBC}	0.0065 m^3 (6.5 L)
reaction volume, V	0.014 m^3 (14 L)
recirculation liquid flow rate, Q_L	2.3×10^{-4} m^3/s (14 L/min)
gas flow rate, Q_G	8.3×10^{-7}, 16.6×10^{-7}, and 25×10^{-7} m^3/s (0.050, 0.10, and 0.15 L/min)
temperature, T	288, 293, 298, 303, and 308 K
pressure, P	101 kPa
inlet power, outlet power UV-CL	400 W, 132 W at λ = 254 nm

4 h (using a heating ramp of 1 °C/min) under air flow prior to the adsorption and heterogeneous photocatalytic tests.

The chemical composition of solids was determined in a Perkin−Elmer model Optima 3200 Dual Vision by inductively coupled plasma−atomic emission spectrometry (ICP-AES).

The band-gap energy (E_g) was determined using a Cary Model 100 spectrophotometer with an integration sphere.

2.3. Heterogeneous Photocatalytic Oxidation of 4CP. In order to establish optimal operating conditions in the CDBC, a hydrodynamic study was carried out with different gas−liquid systems without reaction. The gas−liquid systems consisted of air and 4CP aqueous solutions at different concentrations (0, 2×10^{-4}, 3×10^{-4}, 5×10^{-4}, 6.3×10^{-4}, and 8×10^{-4} kmol/m^3). Experiments were repeated three times to verify the results reliability at 298 K. In all cases, the gas was introduced when the entire column was completely filled with liquid, and liquid circulation was established. The recirculation liquid flow rate (Q_L) was varied in the range of $(1-2.7) \times 10^{-4}$ m^3/s, and the gas flow rate (Q_G) was varied over the range of $(8.3-25) \times 10^{-7}$ m^3/s.

Then, 0.014 m^3 of aqueous solution containing different amounts of 4CP were loaded into the reaction system. After having reached batch loop operation mode, with $Q_L = 2.3 \times 10^{-4}$ m^3/s and a continuous supply of air ($Q_G = 8.3 \times 10^{-7}$ m^3/s), irradiation was started and T was kept constant throughout the experiment. In order to establish the kinetic parameters, the studied variables were T (288, 293, 298, 303, and 308 K), catalyst loading (C_{cat} = 0.40, 0.80, and 1.2 kg/m^3), and 4CP initial concentration ($C_{4CP0} = 3 \times 10^{-4}$, 5×10^{-4}, 6.3×10^{-4}, and 8×10^{-4} kmol/m^3). All liquid samples were centrifuged to remove catalyst before analysis. It is noteworthy that the concentration change of 4CP in the adsorption experiment was negligible (~14% of removal).

Prior reaction, however, the adsorption capacity of calcined solids was determined by recirculating 0.014 m^3 of aqueous solution containing 6.3×10^{-4} kmol/m^3 of 4CP and 0.0113 kg of calcined powders (C_{cat} = 0.80 kg/m^3), with a continuous supply of air. Aliquots were taken from the CDBC every 1800 s during 10 800 s. The temperature throughout the experiment was kept constant at 298 K. All liquid samples were centrifuged to remove catalyst before analysis.

At all experiments, the concentration of 4CP (C_{4CP}) was determined using UV/vis spectroscopy in a Perkin−Elmer Model Lambda 25 UV/vis spectrophotometer with a wavelength range of 190−1100 nm. C_{4CP} is directly proportional to absorbance, according to the Beer−Lambert law,

$$A = \varepsilon b C_{4CP}$$

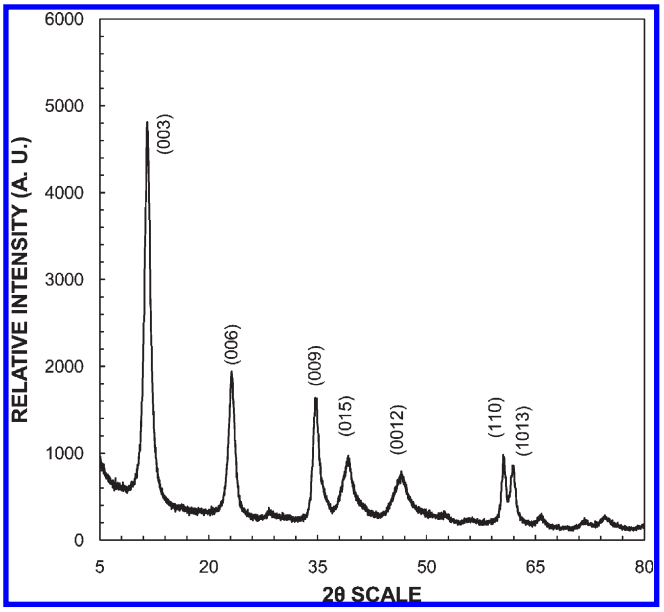

Figure 2. XRD pattern of MgAlZn−5% LDHs.

where A is the absorbance at 280 nm, b the path length, and ε the molar absorptivity coefficient. A calibration curve was constructed from 0 to 8×10^{-4} kmol/m^3, obtaining a coefficient of determination of $r^2 = 0.9989$. The experiments were repeated three times to verify results reliability.

The total organic carbon content (TOC) value was analyzed with an Apollo Model 9000 TOC Analyzer (using catalyzed combustion at 953 K), which monitored the aqueous solution after centrifugation directly.

3. RESULTS AND DISCUSSION

3.1. Catalyst Characterization. A complete characterization of the as-synthesized-here catalytic precursor has been previously presented,[13] and a specific surface area of the calcined powders of 255 m^2/g and a pore diameter of 18 nm have been reported. Nevertheless, XRD analysis was conducted in order to ensure the presence of pure hydrotalcite-like phase in MgAlZn−5% LDHs powders synthesized by coprecipitation at constant pH.

The XRD pattern of the as-synthesized solid, displayed in Figure 2, corresponds to that of a pure LDH. This pattern is characterized by strong, harmonic 001 reflections at low 2θ values, and weaker in-plane reflections at higher angles. The interlayer distance is reflected by the unit-cell parameter c, while the parameter a corresponds to the average cation−cation distance, assuming a 3R stacking pattern. These parameters were calculated by the position of the 003 and 110 peaks, respectively. The interlayer distance (c = 22.911 Å) was found to have good agreement with that of the intercalation carbonate anions. The average cation−cation distance (a = 3.065 Å), follows Vegard's law for solid solutions, and corresponds well to the chemical composition determined by ICP-AES.[19] Accordingly, the general formula for the MgAlZn−5% LDH is $[Mg_{0.61}Al_{0.33}Zn_{0.06}(OH)_2](CO_3)_{0.165}\ H_2O$.

The band-gap energy (E_g) of the MgAlZn−5% LDH, determined via diffuse reflectance UV/vis spectroscopy (see Figure 3), was determined to be of 5.43 eV. This value is relatively high, when compared to that of anatase, which has $E_g \approx 3.0$ eV.

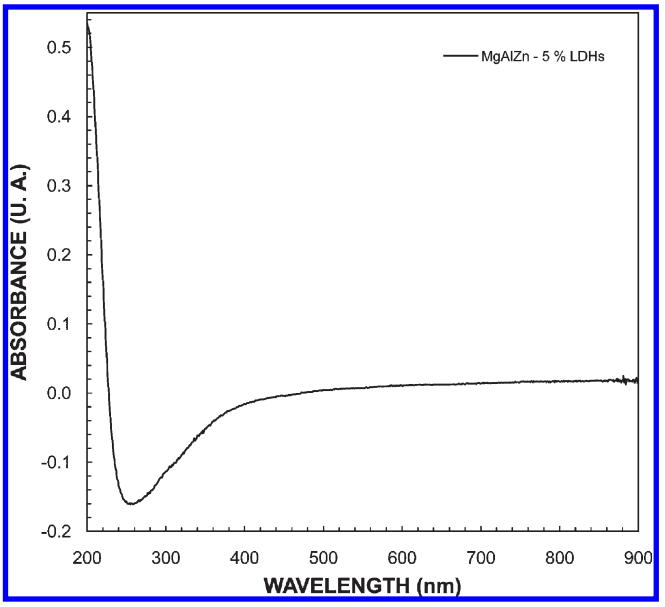

Figure 3. UV/vis absorbance spectrum of MgAlZn−5% LDH, used for determination of the band-gap energy (E_g).

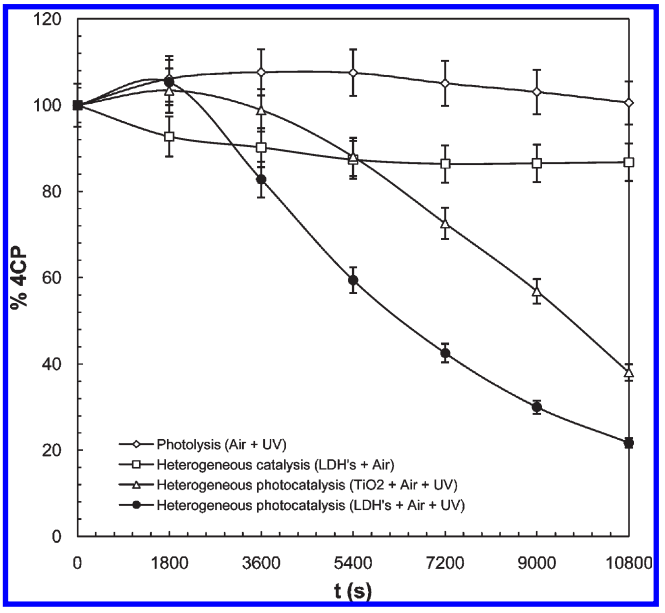

Figure 4. Effect of catalyst type, photolysis, and adsorption on the amount (percentage) of removed 4CP as a function of time. Conditions: T = 298 K, P = 101 kPa, $Q_G = 8.3 \times 10^{-7}$ m^3/s, and C_{cat} = 0.80 kg/m^3 (0.8%) (except for photolysis).

3.2. 4CP Degradation. According with the hydrodynamic study, regardless of the gas−liquid system (i.e., at different 4CP concentrations and, thus, different bubble sizes), the pattern of the gas−liquid dispersion and the process of bubbles formation were observed. It was found that $Q_L = 2.3 \times 10^{-4}$ m^3/s was sufficient to prevent the formation of a gas pocket at the top of the column for each analyzed Q_G. Moreover, a Q_G value of 8.3×10^{-7} m^3/s was found to be adequate to maintain a stable bubble dispersion without the formation of a gas pocket on the CDBC top. When Q_G was increased, a gas pocket appeared in the

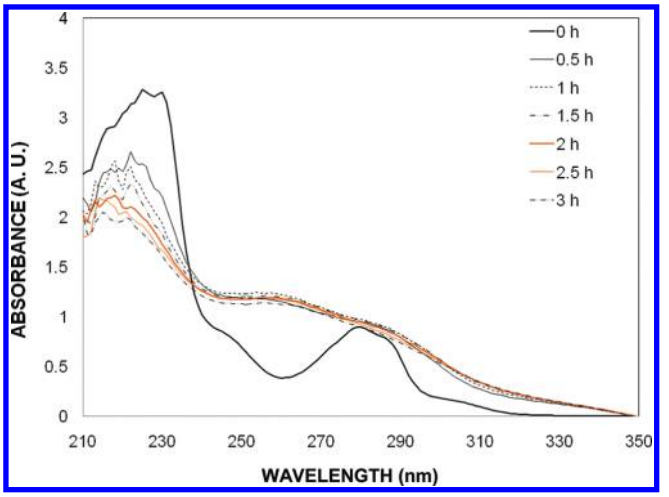

Figure 5. UV/vis spectra of the 4CP degradation under photolysis. Conditions: $C_{4CP0} = 6.3 \times 10^{-4}$ kmol/m^3, T = 298 K.

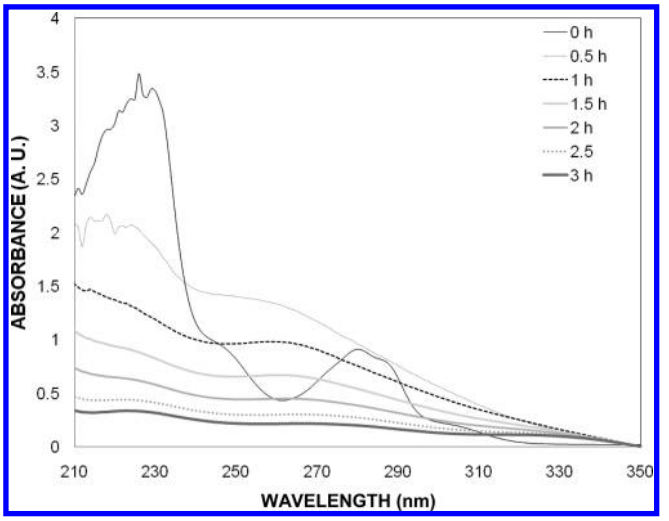

Figure 6. UV/vis spectra of the catalyzed photodegradation of 4CP by MgAlZn−5% LDH. Conditions: $C_{4CP0} = 6.3 \times 10^{-4}$ kmol/m^3, T = 298 K.

expansion zone of the reactor. Because of the above-mentioned information, the 4CP photodegradation experiments were performed with Q_L values 2.3×10^{-4} m^3/s and Q_G values of 8.3×10^{-7} m^3/s.

The effect of catalyst type and photolysis on 4CP degradation was studied. It can be observed in Figure 4, which shows the remaining amount (percentage) of 4CP as a function of irradiation time under various reaction conditions. The effect of photolysis was studied by carrying out the experiment only in the presence of air and UV light without catalyst. From Figure 4, it is evident that the degradation of 4CP by direct photolysis is negligible. Actually, a slight increase in the organic compound concentration is observed during the first 2 h of reaction (see Figures 4 and 5). This, however, is not a real increase in concentration but an electronic effect that modifies the UV absorbance spectrum and appears as if it was an increase in concentration.[16] This phenomenon has been observed to occur with other LDH compounds[16] and has been described as a photoinduction period associated with reactions involving the formation of free radicals.[13,16,20] Nevertheless, according to other

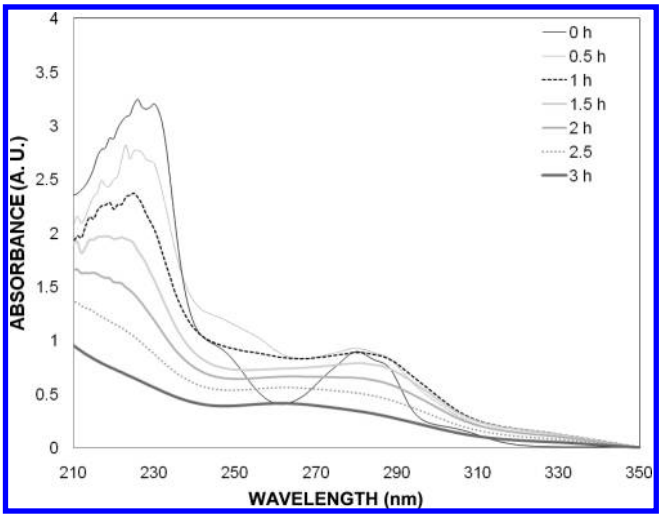

Figure 7. UV/vis spectra of the catalyzed photodegradation of 4CP by Degussa P25. Conditions: $C_{4CP0} = 6.3 \times 10^{-4}$ kmol/m^3, $T = 298$ K.

reports,[21] the 4CP degradation readily occurs under UV light and air, since the *in situ* production of oxidant compounds (such as H_2O_2) occurs. The production rate of such compounds has been evidenced to be pH-dependent and highly favored in acidic media.[21] However, in this work, a basic pH was observed during the entire photolytic experiment, which may explain the absence of 4CP degradation under photolysis. A similar photoinduction period was observed when using either calcined MgAlZn−5% LDHs (Figure 6) or Degussa P25 (TiO_2) (Figure 7). In these cases, however, the photoinduction periods are different in length, being shorter for the calcined MgAlZn−5% LDHs (~0.5 h) than for Degussa P25 (~1 h). This difference could be ascribed to a larger number of hydroxyl species in the calcined MgAlZn−5% LDH than in Degussa P25.[16,20] Such surface basic group has been suggested[15] to be associated with the production of a charge-transfer complex[16,22−24] before the generation of hydroxyl radicals is sufficient to initiate 4CP degradation. Figure 4 indicates that such generation is faster with the MgAlZn−5% LDHs than with Degussa P25. For the former, an initial reaction rate of 6.17×10^{-8} kmol/(kg$_{cat}$ s) was calculated, whereas for the latter, it was 1.58×10^{-8} kmol/(kg$_{cat}$ s). This significant difference may be questionable, from a physical point of view, if one considers the E_g for each material. For the anatase TiO_2, $E_g \approx 3.2$ eV, whereas, for the MgAlZn−5% LDHs, $E_g \approx 5.43$ eV (Figure 3). These values indicate that the feasibility of producing an (h^+_{VB}/e^-_{CB}) pair is higher in the TiO_2 than in the LDH compound. However, it could also be that, because of a shorter E_g the ease of h^+_{VB}/e^-_{CB} recombination is also higher in the Degussa P25 compound than in the MgAlZn−5% LDH compound. Thus, at the beginning of irradiation, even when the number of (h^+_{VB}/e^-_{CB}) pairs is higher in the TiO_2, it could be that their "lifetime" is shorter than those pairs produced in the MgAlZn−5% LDH compound. Hence, the probability of water molecules finding available h^+_{VB} to adsorb and produce oxidant species by reaction 1[2] would be higher in the MgAlZn−5% LDH compound.

$$\text{oxide}(h^+_{VB}) + (H_2O)_{ad} \rightarrow \text{oxide} + (HO\bullet)_{ad} + H^+ \quad (1)$$

In Degussa P25, the shorter E_g could be favoring not only direct recombination of h^+_{VB}/e^-_{CB} pairs (reaction 2) but also the reduction of adsorbed hydroxyl radicals by conduction-band electrons (reaction 3):

$$TiO_2\ (h^+_{VB} + e^-_{CB}) \rightarrow TiO_2 + \text{heat} \quad (2)$$

$$TiO_2\ (e^-_{CB}) + (HO\bullet)_{ad} \rightarrow TiO_2 + (HO^-)_{ad} \quad (3)$$

Thus, limiting not only reaction 1 but also reaction 4,

$$(HO\bullet)_{ad} + (\text{compounds})_{ad} \rightarrow \text{oxidized products} \quad (4)$$

Table 2 summarizes the main differences found between the calcined LDH and Degussa P25.

3.2.1. Kinetic Study. Once the calcined MgAlZn−5% LDH compound was proven as a potential catalyst for the 4CP photodegradation, a more-detailed kinetic study was conducted. According to the literature,[25,26] 4CP degradation rate is dependent on C_{4CP}, the oxygen molecular concentration, ionic strength, C_{cat}, incident radiation, and reactor design. In this work, the effect of C_{4CP0} on its degradation rate was studied in the range of $(3-8) \times 10^{-4}$ kmol/m^3. For such a purpose, C_{4CP} profiles were produced from different C_{4CP0} values. These profiles are shown in Figure 8, where it is interesting to observe that the photoinduction period length is a function of C_{4CP0}. It is evident that such period is shorter at lower C_{4CP0}. This fact supports the statement regarding the initial production of a charge-transfer complex between the phenolic compound and the catalytic surface. It could be that, at this point, photolysis rather than photocatalysis rules the degradation process and this may explain the absence of a photoinduction period that has been mainly related to the interaction of the phenolic compounds with the catalytic surface.[16,20,24] This does not mean that there is photolytic degradation of 4CP, since this has been disregarded because of the results shown in Figure 4. However, the photolytic production of hydroxyl radicals has been suggested[26,27] to occur via the following route:

$$e^- + O_2 \rightarrow O_2^- \quad (5)$$

$$O_2^- + H^+ \rightarrow (HO\bullet)_2 \quad (6)$$

$$(HO\bullet)_2 + (HO\bullet)_2 \rightarrow H_2O_2 + O_2 \quad (7)$$

$$H^+ + O_2^- + (HO\bullet)_2 \rightarrow H_2O_2 + O_2 \quad (8)$$

$$H_2O_2 + h\nu \rightarrow 2HO\bullet \quad (9)$$

Therefore, the catalyst role would be not only to generate the h^+_{VB} so that water molecules could adsorb and produce adsorbed hydroxyl radicals via reaction 1, but also to produce electrons that aid in the production of superoxide anions and hydrogen peroxide (reactions 5−9).

In the literature, it is generally acknowledged that a Langmuir−Hinshelwood model (eq 10) that considers one type of sites and the noncompetitive 4CP adsorption[7,13,16] would represent the heterogeneously photocatalyzed 4CP degradation reasonably well.

$$-r_{4CP} = -\frac{dC_{4CP}}{dt} = \frac{k_a K_{4CP} C_{4CP}}{1 + K_{4CP} C_{4CP}} \quad (10)$$

In this equation, $-r_{4CP}$ is the degradation rate of 4CP (in units of kmol/(m^3 s)), k_a the reaction rate constant (in units of kmol/(m^3 s)),

Table 2. Summary of Results Found with the MgAlZn−5% LDH Compound and Degussa P25[a]

catalyst	band-gap (eV)	photoinduction period (s)	4CP degradation rate (kmol/(kg_{cat} s))	removal of 4CP (%)
MgAlZn−5% LDH	5.43	1800	6.17×10^{-8}	80
TiO_2 Degussa P25	3.2	3600	1.57×10^{-8}	60

[a] Conditions: $C_{4CP0} = 6.3 \times 10^{-4}$ kmol/m^3, $T = 298$ K, $P = 101$ kPa, $Q_G = 8.3 \times 10^{-7}$ m^3/s, and $C_{cat} = 0.8$ kg/m^3.

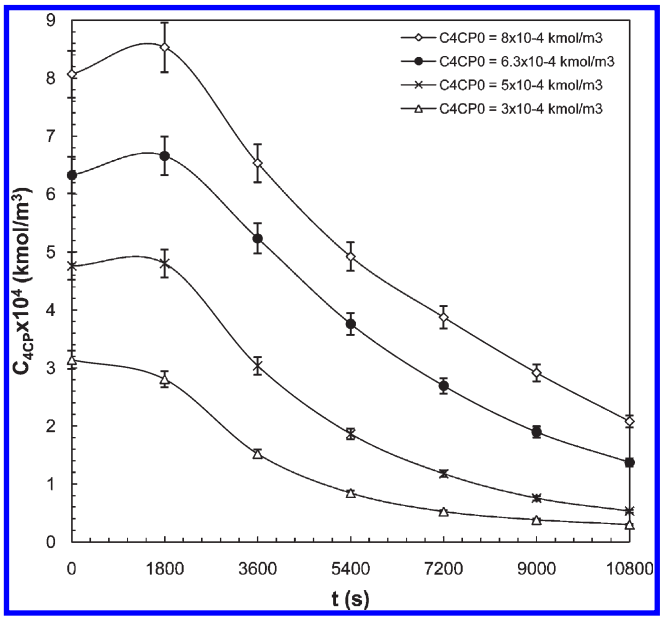

Figure 8. 4CP concentration (C_{4CP}) profiles, as a function of time and C_{4CP0}. Catalyst: calcined MgAlZn−5% LDH, $C_{cat} = 0.80$ kg/m^3, $T = 298$ K.

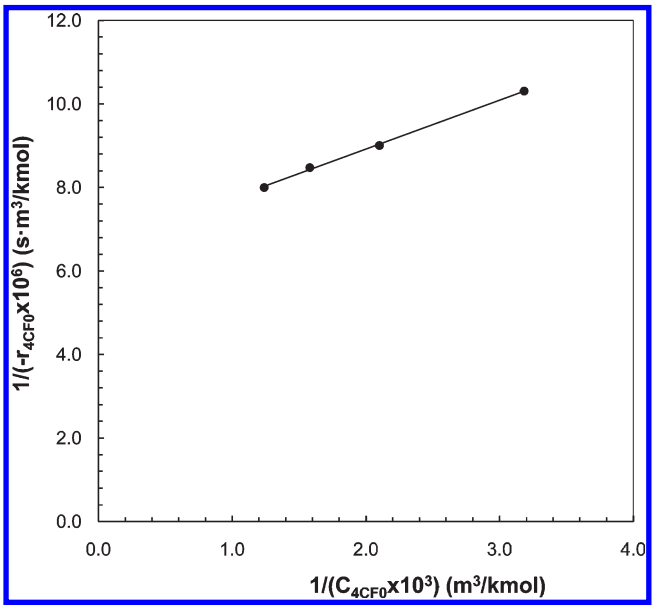

Figure 9. Fitting of experimental data to a single-site Langmuir−Hinshelwood kinetic model.

K_{4CP} the adsorption coefficient of 4CP (in units of m^3/kmol), and C_{4CP} the molar concentration of 4CP.

Thus, in order to verify that the 4CP photodegradation catalyzed by a calcined MgAlZn LDHs compound follows a single-site Langmuir−Hinshelwood mechanism, eq 10 was linearized and the inverse of the initial degradation rate of 4CP ($-r_{4CP0}$) was plotted in Figure 9 as a function of the inverse of C_{4CP0}. An excellent fitting ($r^2 = 0.99$) was found in the studied concentration range. From the slope and intercept of this plot, k_a and K_{4CP} were estimated; their values are 1.52×10^{-7} k mol/(m^3 s) and 5.6×10^3 m^3/kmol, respectively. The comparison of these values with those reported in the literature could seem futile for a moment, since they are strongly dependent on the experimental conditions. Moreover, there are no reported values of these constants for the 4CP degradation photocatalyzed by the calcined MgAlZn LDH compound employed. One also should remember that catalyst concentration, incident radiation (absorbed photons), and reactor design play a major role in photoconversion rate. Actually, the reaction rate of photocatalytic processes can generally be expressed as

$$r = f(C_{i0})f(C_{cat})f(P_a)$$

where C_{i0} is the initial reactant concentration and P_a the number of absorbed photons. In this study, when catalyst loading was kept constant, it could be assumed that the amount of absorbed photons was also constant. When catalyst loading is increased, however, the absorbed photons will also increase and thus photoconversion rate (r) will increase until reaching a maximum. Beyond this point, the further addition of catalyst would be useless. As long as the relationship between photoconversion rate and catalyst concentration and photons absorption is kept linear (low levels of absorbed incident radiation), the effect of both variables, catalyst concentration, and photons absorption (when kept constant), can be enclosed in the photoconversion rate constant (k_a). Hence, any variable affecting either catalyst concentration or photons absorption will affect k_a. At this point, it is worth mentioning that reactor design importantly affects the incident radiation, because of the lamp position (inside or outside the reactor), irradiated volume, and construction material transparency.

Also, it is worth noticing that this research is the first carried out with the aforementioned catalyst and at pilot scale. Hence, in order to position this work in the general photocatalyzed 4CP degradation context, Table 3 presents some k_a and K_{4CP} values reported with other catalysts and at laboratory scale. Although the literature concerning photocatalyzed 4CP degradation is vast, only few research groups report values for the aforementioned constants.

3.2.2. Effect of Temperature. Generally speaking, various studies[25,30,31] have been performed to elucidate the dependence of TiO_2 activity with temperature, and none has been conducted with the catalyst used in this work. All of them concurred in stating that, although low temperature does not activate TiO_2, its dependency with temperature is worth exploring, in view of solar applications. In addition, in this work, the reaction rate temperature dependence was considered worthy to explore, since the UV lamp itself represents a source of heat.

Table 3. Reaction and Adsorption Constants (k_a and K_{4CP}, Respectively) Reported in This Work and in the Literature

catalyst	k_a (kmol/(m^3 s))	K_{4CP} (m^3/kmol)	T (K)	V (m^3)	reference
MgAlZn−5% LDH	1.52×10^{-7}	5.6×10^3	298	0.014	this work
Hombikat UV 100	5.56×10^{-8}	2.4×10^4	293	150×10^{-6}	25
TiO_2 Degussa P25		1.66×10^4, 1.9×10^4	293		28, 29

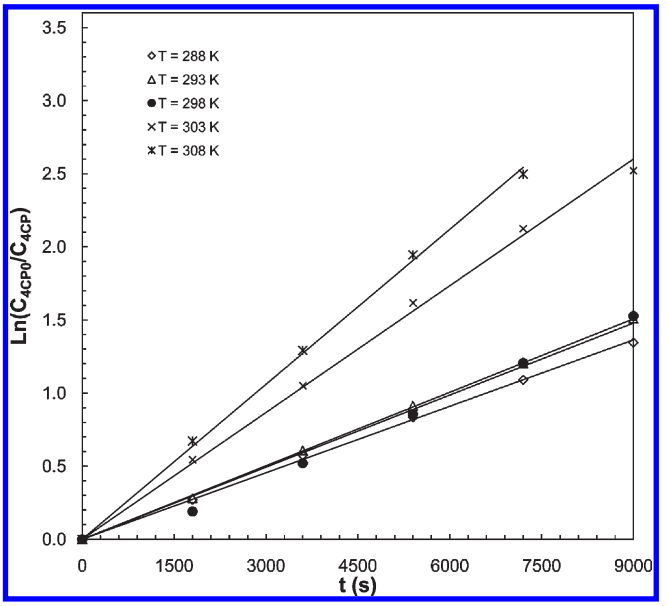

Figure 10. Effect of temperature over first-order apparent kinetic constant.

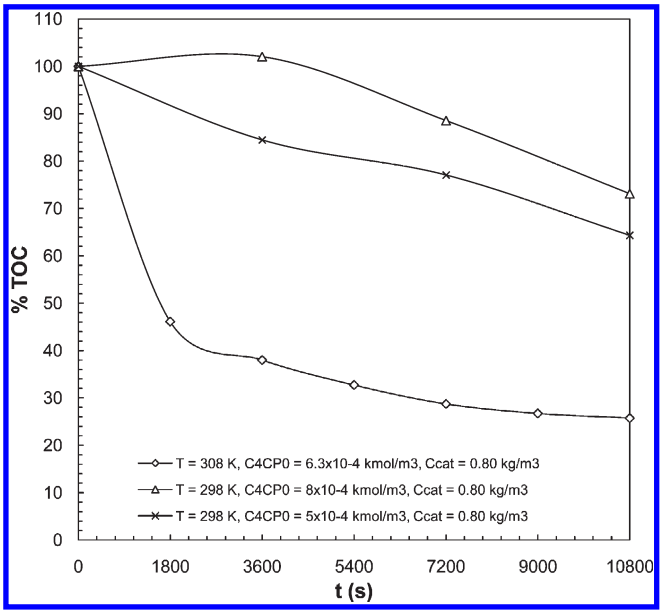

Figure 11. Effect of temperature and initial 4CP concentration (C_{4CP0}) on the total organic carbon content (TOC) reduction percentage.

Table 4. Apparent Kinetic Constant at Different Temperature

$k_{ap} \times 10^4$ (kmol/(m^3 s))	temperature, T (K)	r^2
1.5143	288	0.99
1.6416	293	0.98
1.6748	298	0.99
2.8883	303	0.99
3.5319	308	0.99

The effect of this thermodynamic variable was systematically studied in the range of 288−308 K. For this study, the $C_{4CP0} = 6.3 \times 10^{-4}$ kmol/m^3. Figure 10 depicts the obtained experimental data fitted to a pseudo-first-order reaction model (eq 11):

$$-r_{4CP} = k_{ap} C_{4CP} \quad (11)$$

This equation is obtained by assuming that the adsorption term in eq 10 is relatively small, compared to 1, because either the adsorption constant or the 4CP concentration on the surface is relatively low. The temperature dependence of reaction rate is given by the apparent reaction constant, k_{ap} (slope). It can be observed that the reaction rate increases when increasing temperature since the k_{ap} value increases accordingly (see Table 4). However, there is not a linear trend and this is typical behavior when Langmuir−Hinshelwood-type kinetics dominates the process. It is well-known that adsorption is an inverse function of temperature. This also applies to photocatalysts such as TiO_2, even at low temperature.[31] For such a catalyst, its photocatalytic activity has been reported to be drastically reduced with temperature, as a consequence of decreased organic compound adsorption and, therefore, surface coverage. It is worth noting that this behavior was not observed with the catalyst under study (see Figure 10). This could be ascribed to a change in controlling mechanism step and the catalytic surface role. Although all the same reactions (reactions 1−9) may be occurring and while some of them are not favored by temperature, there are others (reactions 7 and 8) that have been reported[27] to be positively affected by such a variable.

Figure 11 shows the effect of temperature and C_{4CP0} on TOC percentage. The effect of both variables is observed to be significant, mainly on oxidation rate and final TOC content. These results support the aforementioned regarding the correlation of organic compounds adsorption with T and C_{4CP0}. It can also be observed that TOC was not completely reduced, and this indicates an incomplete mineralization of the model pollutant. HPLC, LC-MS, and GC-MS techniques allow the determination of reaction intermediates. Although interesting, such characterization is beyond the scope of this paper. In specialized literature, however, hydroquinone (HQ), benzoquinone (BQ), and 4-chlorocatechol (4CC) have been reported as the major aromatic intermediates, which are also toxic. One should bear on mind that these intermediates have been obtained with other catalysts as TiO_2.[21,25]

Finally, the effect of C_{cat} on C_{4CP} profiles was investigated in the range of 0.4−1.2 kg/m^3. The results are shown in Figure 12. Evidently, the 4CP photodegradation rate significantly increases accordingly with C_{cat}. This suggests that the degradation process

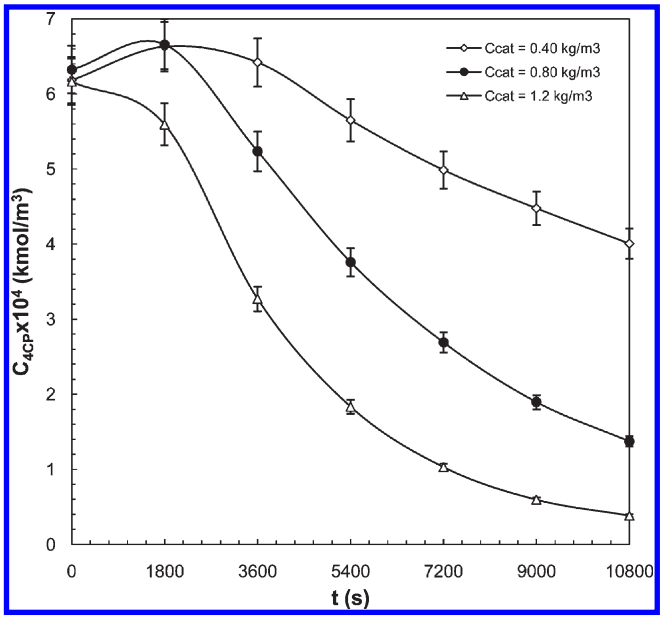

Figure 12. Effect of catalyst loading (C_{cat}) on concentration profiles. Conditions: $C_{4CP0} = 6.3 \times 10^{-4}$ kmol/m^3, $T = 298$ K.

was carried out under an intrinsic kinetic regime.[30−32] Actually, the internal diffusion resistance could have been discarded from the very beginning, since the particle size of the employed catalyst was 10 μm (determined by light scattering technique). In Figure 12, it is also noticeable that, with a C_{cat} value as small as 0.12%, a 4CP degradation of 94% is achieved. Moreover, the photoinduction period is reduced when C_{cat} is increased. This may be ascribed once again to the number ratio of organic compound molecules to active sites. This would be lowest at the highest catalyst concentration.

CONCLUSIONS

4-Chlorophenol (4CP) photodegradation catalyzed by a MgAlZn mixed oxide obtained via the calcination of a layered double hydroxide (LDH) precursor was studied for the first time at pilot scale in a bubble column. The employed catalyst was found to provide a faster degradation rate than Degussa P25. Among the studied variables, temperature was determined to be the one that affects both the total organic carbon content (TOC) and photodegradation rate the most. The photodegradation process was found to be controlled by a single-site Langmuir−Hinshelwood-type mechanism. Thus, to optimize the rate of photodegradation and the degree of mineralization, the surface coverage with the organic compound also must be optimized, either by changing the 4CP concentration or temperature. In the range of studied operating conditions, maximums of 94% 4CP degradation and 70% TOC removal were attained.

AUTHOR INFORMATION

Corresponding Author

*Tel.: +52 (722) 2 76 66 10, Ext. 7723. Fax: +52 (722) 2 17 38 90. E-mail: reynanr@gmail.com.

Present Addresses

$^{\perp}$Centro Conjunto de Investigación en Química Sustentable, Facultad de Química, Universidad Autónoma del Estado de México, Km 14.5 Carretera Toluca-Atlacomulco, México.

REFERENCES

(1) Pera-Titus, M.; García-Molina, V.; Baños, M. A.; Giménez, J.; Esplugas, S. Degradation of chlorophenols by means of advanced oxidation processes: a general review. *Appl. Catal., B* **2004**, *47* (4), 219–256.

(2) Bauer, R.; Waldner, G.; Fallmann, H.; Hager, S.; Klare, M.; Krutzler, T.; Malato, S.; Maletzky, P. The photo-Fenton reaction and the TiO_2/UV process for waste water treatment—Novel developments. *Catal. Today* **1999**, *53* (1), 131–144.

(3) Boyes, A. P.; Chughtai, A.; Lu, X. X.; Raymahasay, S.; Sarmento, S.; Tilston, M. W.; Winterbottom, J. M. The cocurrentdownflow contactor (CDC) reactor-chemically enhanced mass transfer & reaction studies for slurry and fixed bed catalytic hydrogenation. *Chem. Eng. Sci.* **1992**, *47* (13−14), 3729–3736.

(4) Lu, X.-X.; Boyes, A. P.; Winterbottom, J. M. Operating and hydrodynamic characteristics of a cocurrentdownflow bubble column reactor. *Chem. Eng. Sci.* **1994**, *49* (24, Part 2), 5719–5733.

(5) Ochuma, I. J.; Fishwick, R. P.; Wood, J.; Winterbottom, J. M. Optimisation of degradation conditions of 1,8-diazabicyclo[5.4.0]undec-7-ene in water and reaction kinetics analysis using a cocurrentdownflow contactor photocatalytic reactor. *Appl. Catal., B* **2007**, *73* (3−4), 259–268.

(6) Winterbottom, J. M.; Khan, Z.; Raymahasay, S.; Knight, G.; Roukounakis, N. A comparision of tryglyceride oil hydrogenation in a downflow bubble column using slurry and fixed bed catalysts. *J. Chem. Technol. Biotechnol.* **2000**, *75* (11), 1015–1025.

(7) Natividad, R.; Cruz-Olivares, J.; Fishwick, R. P.; Wood, J.; Winterbottom, J. M. Scaling-out selective hydrogenation reactions: From single capillary reactor to monolith. *Fuel* **2007**, *86* (9), 1304–1312.

(8) Fishwick, R. P.; Natividad, R.; Kulkarni, R.; McGuire, P. A.; Wood, J.; Winterbottom, J. M.; Stitt, E. H. Selective hydrogenation reactions: A comparative study of monolith CDC, stirred tank and trickle bed reactors. *Catal. Today* **2007**, *128* (1−2), 108–114 (Special Issue).

(9) Lu, X.-X.; Boyes, A. P.; Winterbottom, J. M. Study of mass transfer characteristics of a cocurrent downflow bubble column reactor using hydrogenation of itaconic acid. *Chem. Eng. Sci.* **1996**, *51* (11), 2715–2720.

(10) Ochuma, I. J.; Fishwick, R. P.; Wood, J.; Winterbottom, J. M. Photocatalytic oxidation of 2,4,6-trichlorophenol in water using a cocurrent downflow contactor reactor (CDCR). *J. Hazard. Mater.* **2007**, *144* (3), 627–633.

(11) Ochuma, I. J.; Osibo, O. O.; Fishwick, R. P.; Pollington, S.; Wagland, A.; Wood, J.; Winterbottom, J. M. Three-phase photocatalysis using suspended titania and titania supported on a reticulated foam monolith for water purification. *Catal. Today* **2007**, *128* (1−2), 100–107.

(12) Winterbottom, J. M.; Khan, Z.; Boyes, A. P.; Raymahasay, S. Photocatalyzed oxidation of phenol in water using a concurrent downflow contactor reactor (CDCR). *Environ. Prog.* **1997**, *16* (2), 125–131.

(13) Valente, J. S.; Tzompantzi, F.; Prince, J.; Cortez, J. G. H.; Gomez, R. Adsorption and photocatalytic degradation of phenol and 2,4-dichlorophenoxiacetic acid by Mg-Zn-Al layered double hydroxides. *Appl. Catal., B* **2009**, *90* (3−4), 330–338.

(14) Mantilla, A.; Tzompantzi, F.; Fernández, J. L.; Diaz Góngora, J. A. I.; Gómez, R. Photodegradation of 2,4-dichlorophenoxyacetic acid using ZnAlFe layered double hydroxides as photocatalysts. *Catal. Today* **2009**, *148* (1−2), 119–123.

(15) Mantilla, A.; Tzompantzi, F.; Fernández, J. L.; Diaz Góngora, J. A. I.; Gómez, R. Photodegradation of phenol and cresol in aqueous medium by using Zn/Al + Fe mixed oxides obtained from layered double hydroxides materials. *Catal. Today* **2010**, *150* (3−4), 353–357.

(16) Valente, J. S.; Tzompantzi, F.; Prince, J. Highly efficient photocatalytic elimination of phenol and chlorinated phenols by CeO_2/MgAl Layered Double Hydroxides. *Appl. Catal., B* **2011**, *102* (1−2), 276–285.

(17) Liotta, L. F.; Gruttadauria, M.; Di Carlo, G.; Perrini, G.; Librando, V. Heterogeneous catalytic degradation of phenolic substrates: Catalysts activity. *J. Hazard. Mater.* **2009**, *162* (2−3), 588–606.

(18) Patzkó, A.; Kun, R.; Hornok, V.; Dékány, I.; Engelhardt, T.; Schall, N. ZnAl-layer double hydroxides as photocatalysts for oxidation of phenol in aqueous solution. *Colloid. Surf. A* **2005**, *265* (1−3), 64–72.

(19) Cavani, F.; Tifirò, F.; Vaccari, A. Hydrotalcite-type anionic clays: Preparation, properties and applications. *Catal. Today* **1991**, *11* (2), 173–301.

(20) Sivalingam, G.; Priya, M. H.; Madras, G. Kinetics of the photodegradation of substituted phenols by solution combustion synthesized TiO_2. *Appl. Catal., B* **2004**, *51* (1), 67–76.

(21) Du, Y.; Fu, Q. S.; Li, Y.; Su, Y. Photodecomposition of 4-chlorophenol by reactive oxygen species in UV/air system. *J. Hazard. Mater.* **2011**, *186*, 491−496.

(22) Wang, N.; Zhu, L.; Huang, Y.; She, Y.; Yu, Y.; Tang, H. Drastically enhanced visible-light photocatalytic degradation of colorless aromatic pollutants over TiO_2 via a charge-transfer-complex path: A correlation between chemical structure and degradation rate of the pollutants. *J. Catal.* **2009**, *266* (2), 199–206.

(23) Agrios, A. G.; Gray, K. A.; Weitz, E. Photocatalytic Transformation of 2,4,5-Trichlorophenol on TiO_2 under Sub-Band-Gap Illumination. *Langmuir* **2003**, *19* (12), 5178–5178.

(24) Agrios, A. G.; Gray, K. A.; Weitz, E. Narrow-Band Irradiation of a Homologous Series of Chlorophenols on TiO_2: Charge-Transfer Complex Formation and Reactivity. *Langmuir* **2004**, *20* (14), 5911–5917.

(25) Theurich, J.; Lindner, M.; Bahnemann, D. W. Photocatalytic Degradation of 4-Chlorophenol in Aerated Aqueous Titanium Dioxide Suspensions: A Kinetic and Mechanistic Study. *Langmuir* **1996**, *12* (26), 6368–6376.

(26) de Lasa, H.; Serrano, B.; Salaices, M. *Photocatalytic Reaction Engineering*, 1st ed.; Springer: London, 2004; p 187.

(27) García Einschlag, F.; Féliz, M. R.; Capparelli, A. L. Effect of temperature on hydrogen peroxide photolysis in aqueous solutions. *J. Photochem. Photobiol. A: Chem* **1997**, *110* (3), 235–242.

(28) Al-Sayyed, G.; D'Olveira, J. C.; Pichat, P. Semiconductor-sensitized photodegradation of 4-chlorophenol in water. *J. Photochem. Photobiol. A: Chem.* **1991**, *58* (1), 99.

(29) Al-Ekabi, H.; Serpone, N.; Pelizzetti, E.; Minero, C.; Fox, M. A.; Draper, R. B. Kinetic studies in heterogeneous photocatalysis. 2. Titania-mediated degradation of 4-chlorophenol alone and in a three-component mixture of 4-chlorophenol, 2,4-dichlorophenol, and 2,4,5-trichlorophenol in air-equilibrated aqueous media. *Langmuir* **1989**, *5* (1), 250–255.

(30) Gaya, U. I.; Abdullah, A. H. Heterogeneous photocatalytic degradation of organic contaminants over titanium dioxide: A review of fundamentals, progress and problems. *J. Photochem. Photobiol. C* **2008**, *9* (1), 1–12.

(31) Herrmann, J.-M. Heterogeneous photocatalysis: fundamentals and applications to the removal of various types of aqueous pollutants. *Catal. Today* **1999**, *53* (1), 115–129.

(32) Chong, M. N.; Jin, B.; Chow, C. W. K.; Saint, C. Recent developments in photocatalytic water treatment technology: A review. *Water Res.* **2010**, *44* (10), 2997–3027.